ENVIRONMENTAL RESEARCH
LETTERS

LETTER • OPEN ACCESS

Similar patterns of tropical precipitation and circulation changes under solar and greenhouse gas forcing

To cite this article: Stergios Misios *et al* 2021 *Environ. Res. Lett.* **16** 104045

View the article online for updates and enhancements.

You may also like

- Possible causes of the Central Equatorial African long-term drought
Wenjian Hua, Liming Zhou, Haishan Chen et al.
- Tropical Pacific cold tongue mode triggered by enhanced warm pool convection due to global warming
Ning Jiang and Congwen Zhu
- Evolution mechanism of principal modes in climate dynamics
Yongwen Zhang, Jingfang Fan, Xiaoteng Li et al.

This content was downloaded from IP address 155.198.10.231 on 27/10/2021 at 14:49

ENVIRONMENTAL RESEARCH
LETTERS



OPEN ACCESS

RECEIVED
9 November 2020

REVISED
19 September 2021

ACCEPTED FOR PUBLICATION
21 September 2021

PUBLISHED
12 October 2021

Original content from this work may be used under the terms of the Creative Commons Attribution 4.0 licence.

Any further distribution of this work must maintain attribution to the author(s) and the title of the work, journal citation and DOI.



LETTER

Similar patterns of tropical precipitation and circulation changes under solar and greenhouse gas forcing

Stergios Misios[1,2,*], Matthew Kasoar[3], Elliott Kasoar[3,4], Lesley Gray[5,6], Joanna Haigh[3], Stavros Stathopoulos[2], Konstantinos Kourtidis[2], Gunnar Myhre[7], Dirk Olivié[8], Drew Shindell[9] and Tao Tang[10]

[1] Department of Geoscience, Aarhus University, Aarhus, Denmark
[2] Department of Environmental Engineering, Democritus University of Thrace, Xanthi, Greece
[3] Department of Physics, Imperial College London, London, United Kingdom
[4] University of Cambridge, Cambridge, United Kingdom
[5] Department of Physics, Oxford University, Oxford, United Kingdom
[6] National Centre for Atmospheric Science, Oxford, United Kingdom
[7] CICERO Center for International Climate and Environmental Research in Oslo, Oslo, Norway
[8] Norwegian Meteorological Institute, Oslo, Norway
[9] Nicholas School of the Environment, Duke University, Durham, NC, United States of America
[10] School of Environment, Yale University, New Haven, CT, United States of America
[*] Author to whom any correspondence should be addressed.

E-mail: stergios@geo.au.dk

Keywords: solar forcing, GHG forcing, PDRMIP, CESM last millennium

Supplementary material for this article is available online

Abstract

Theory and model evidence indicate a higher global hydrological sensitivity for the same amount of surface warming to solar as to greenhouse gas (GHG) forcing, but regional patterns are highly uncertain due to their dependence on circulation and dynamics. We analyse a multi-model ensemble of idealized experiments and a set of simulations of the last millennium and we demonstrate similar global signatures and patterns of forced response in the tropical Pacific, of higher sensitivity for the solar forcing. In the idealized simulations, both solar and GHG forcing warm the equatorial Pacific, enhance precipitation in the central Pacific, and weaken and shift the Walker circulation eastward. Centennial variations in the solar forcing over the last millennium cause similar patterns of enhanced equatorial precipitation and slowdown of the Walker circulation in response to periods with stronger solar forcing. Similar forced patterns albeit of considerably weaker magnitude are identified for variations in GHG concentrations over the 20th century, with the lower sensitivity explained by fast atmospheric adjustments. These findings differ from previous studies that have typically suggested divergent responses in tropical precipitation and circulation between the solar and GHG forcings. We conclude that tropical Walker circulation and precipitation might be more susceptible to solar variability rather than GHG variations during the last-millennium, assuming comparable global mean surface temperature changes.

1. Introduction

In response to surface warming caused by a radiative forcing agent, global precipitation increases at an almost fixed rate of about 2.4%–2.6% degree^{-1} of global warming, independently of the nature of the agent (Andrews *et al* 2010, O'gorman *et al* 2012, Allan *et al* 2020). This temperature dependent increase in precipitation is commonly referred to as the slow component of the apparent (total) hydrological sensitivity, to differentiate from the rapid component, often of opposite sign, associated with near-instantaneous changes in the atmospheric energy budget and properties (Bala *et al* 2010, Myhre *et al* 2018). For the same forcing agent, climate models show substantially different apparent hydrological sensitivities, ascribed mainly to structural model uncertainties in simulating the rapid atmospheric adjustments. For different forcing agents, the apparent hydrological sensitivity strongly depends

© 2021 The Author(s). Published by IOP Publishing Ltd

on atmospheric absorption that stabilizes the atmosphere. For example, model simulations have broadly identified higher hydrological sensitivity for increasing total solar irradiance (TSI) than CO_2 concentrations (Allen and Ingram 2012, Flaschner *et al* 2016, Samset *et al* 2016), attributed to the fact that extra CO_2 in the atmosphere increases atmospheric absorption of shortwave and longwave radiation, stabilizes the atmosphere and reduces the amount of precipitation on short time scales (days to weeks). This mechanism is not effective in the case of increasing TSI, which is a driver that predominately warms the surface.

While global precipitation change is relatively constrained, regional patterns of forced responses are highly uncertain as they depend on dynamics, which are sensitive to model biases (Bony *et al* 2013, He and Soden 2015, Zhang and Soden 2019). Model simulations considering historical or idealized increases in greenhouse gas (GHG) concentrations have identified forced responses in tropical precipitation characterized by wet-get-wetter and dry-get-drier patterns (Held and Soden 2006, Chou *et al* 2009). In a warming climate, most model simulations indicate that the Walker circulation slows down due to thermodynamic and energy budget constraints (Collins *et al* 2010) but some studies indicate no change or even strengthening of the Walker circulation (Kohyama *et al* 2017), consistent with a strengthening trend observed in recent decades (L'heureux *et al* 2013). Past efforts to understand the tropical Pacific response to GHG forcing have identified several competing mechanisms related to ocean dynamics, atmosphere–ocean interactions, sensitivity of atmospheric stability to radiative cooling and global constraints on the hydrological cycle (Clement *et al* 1996, Gu and Philander 1997, Held and Soden 2006, He and Soden 2015). These mechanisms likely operate on different spatial or temporal scales (Chung *et al* 2019, Heede *et al* 2020) thus shaping tropical precipitation and circulation from decadal to centennial and millennial time scales (Dinezio *et al* 2011).

Our understanding on the mechanisms constraining the past, current and future variability of the tropical precipitation and circulation could be improved by studying responses to different forcings in idealized modelling studies (Huneeus *et al* 2014, Samset *et al* 2016). Liu *et al* (2013) compared signatures of TSI versus GHG forcing and identified divergent patterns of tropical precipitation in the last millennium. They showed that increasing TSI caused an increased zonal temperature gradient and reduced precipitation in the tropical Pacific, while increasing GHGs caused an opposite response. These results are in line with evidence for a basin-wide cooling in the equatorial Pacific in periods of increased solar activity on decadal and centennial time scales (Mann *et al* 2009, Meehl *et al* 2009). Observational evidence over the last 60 years, however, has supported the notion of weakened Walker circulation during periods of increased solar cycle activity that eventually should bring more rainfall towards the central Pacific (Misios *et al* 2019), in a fashion similar to the Pacific response to increasing GHG concentrations (Vecchi *et al* 2006, Dinezio *et al* 2009, Bayr *et al* 2014). Multi-model comparisons conducted within the Precipitation Driver Response Model Intercomparison Project (PDRMIP) provided new insights on the precipitation response to different forcing agents (Myhre *et al* 2016). In idealized forcings scenarios of doubling CO_2 concentrations or increasing TSI by 2%, the regional patterns of precipitation responses were found to be similar, characterized by a wetter equatorial Pacific and reduced precipitation over the maritime continent (Samset *et al* 2016, 2018, Sillmann *et al* 2017). Here we pair the idealized PDRMIP simulations with the last millennium (850–2005) ensemble of the Community Earth System Model (CESM-LME) (Otto-Bliesner *et al* 2015) to identify systematic responses in regional precipitation and circulation to changes in TSI and GHG forcings. We demonstrate similar patterns of forced response, stronger for the solar forcing given equal global mean surface warming, for both the idealized PDRMIP simulations and the more realistic CESM-LME runs. Over the 20th century, the negative adjustments to GHG forcing compensate the slow temperature-dependent increases in precipitation, hindering a robust detection of changes in precipitation and the Walker circulation.

2. Methods

We analyse ensemble mean temperature, precipitation and zonal wind anomalies in coupled simulations from nine PDRMIP climate models: CanESM2, GISS-E2-R, HadGEM2, HadGEM3, IPSL-CM5A, MIROC-SPRINTARS, MPI-ESM, NCAR-CESM1-CAM5, and NorESM1. We make use of experiments that consider the effects of an abrupt (a) doubling CO_2 concentration (PDRMIP-CO_2, hereafter) and (b) 2% increase in TSI (PDRMIP-SOL, hereafter), relative to the unperturbed reference values (which differ between the models). These two scenarios give a very similar global mean temperature warming of about 2.4 K at the end of the 100 years simulated period and multi-model mean apparent hydrological sensitivities of 1.4% K^{-1} and 2.4% K^{-1} for PDRMIP-CO_2 and PDRMIP-SOL respectively (Samset *et al* 2016).

PDRMIP invokes idealized scenarios to reduce forcing uncertainties and facilitate multi-model comparisons, which may not be considered as a realistic representation of observed historical forcings, particularly in regards to solar variability. The PDRMIP-SOL scenario assumes a TSI increase which is approximately 20 times stronger than the observed TSI variation over the 11 year solar cycle (∼0.1%).

Furthermore, the step change has been uniformly applied to all spectral bands, contrary to the observed solar cycle spectral dependence being considerably higher in shorter wavelengths (Haigh 1994, Harder *et al* 2019). PDRMIP models also do not consider the UV–ozone-heating interactions in the stratosphere that would amplify the solar cycle impact on climate via a top-down stratospheric pathway in high latitudes (Gray *et al* 2010), but these appear to have only modest impacts in the tropics (Shindell *et al* 2020). As a result, the strongest atmospheric warming in PDRMIP-SOL is found in the upper troposphere while the stratospheric signal is considerably weaker (supplementary figure 1 (available online at stacks.iop.org/ERL/16/104045/mmedia)). This is opposite to the observed atmospheric temperature response to the 11 year solar cycle, which is characterized by stronger warming in the stratosphere than at the surface because of the UV–ozone feedback (Mitchell *et al* 2015).

To identify the forced surface responses to realistic forcing variations we additionally analyse single forcing runs from CESM-LME considering (a) realistic variations in solar spectral irradiances only (CESM-SOL, four realizations) and (b) GHG concentrations only (CESM-GHG, three realizations) (Otto-Bliesner *et al* 2015). With the CESM-LME simulations we can separate the contribution of solar and GHG forcings to the last millennium and highlight the dominant role of GHG forcing in the last 150 years. We have not included an analysis of the all-forcing runs from CESM-LME because the solar signature would be likely contaminated by the strong volcanic eruptions that have often occurred in periods of grand solar minima. Although the spectral distribution of the imposed changes is more realistic in the CESM-LME simulations they (and also the PDRMIP experiments) nevertheless do not include stratospheric ozone variability and hence the 'top-down' solar cycle mechanisms are under-represented as the solar-induced warming in the stratosphere is muted (supplementary figure 1). However, as detailed in Misios *et al* (2019), this facilitates the attribution of signals to direct TSI forcing of surface warming, although we note that the exclusion of stratospheric ozone feedbacks may increase the modelled sensitivity to the imposed solar forcing as solar radiation reaches the surface unmodulated (Chiodo and Polvani 2016).

3. Results

3.1. Global responses

To focus on the longer time scales, we apply a low-pass six-order Butterworth digital filter with cut-off period at 30 years in the ensemble mean annual time series of PDRMIP-CO_2, PDRMIP-SOL and CESM-GHG, following the methodology of Mann (2004). This filtering, necessitated by the relatively small ensemble size of the runs, efficiently dampens internal variability on decadal and interannual scales—the latter dominated by the El Niño–Southern Oscillation (ENSO) signature. Global mean temperature in CESM-GHG stays relatively stable over the last millennium, with filtered (unfiltered) variations hardly exceeding 0.1 K (0.3 K) and only after 1850 shows a steady increase of 0.07 K decade^{-1}, significantly accelerated to 0.2 K decade^{-1} in the last half of the 20th century (figure 1(b)). Associated with the global surface warming, global precipitation increases by 1.8% in year 2005 relative to the 1850 conditions. In the case of the ensemble mean CESM-SOL time series, we applied a 150 year low-pass Butterworth filter to isolate the centennial component of the climate variability, corresponding to periods of prolonged solar maxima and minima (figure 1(a)). In this way, multidecadal natural variability related to the Pacific Decadal Oscillation (50–70 years) is additionally filtered out. Note that results on centennial time scales are not particularly sensitive to the cut-off period. CESM-SOL simulates a multi-centennial cooling trend over the last millennium, with the coolest period in the filtered and unfiltered global anomalies relative to the 1000–1200 AD of about −0.1 K and −0.2 K, respectively, found coincident to the Maunder Minimum of TSI. The solar induced cooling has approximately the same magnitude of the centennial-scale cooling in other CESM-LME single-forcing runs considering forcings from land use changes or volcanic eruptions (Otto-Bliesner *et al* 2015) and is comparable to the modelled temperature variations prior to 1800 caused by GHG forcing (figure 1). In the post-1700 period, TSI increase contributes to global temperature increase by 0.1 K. The 150 year low pass filtering isolates global mean surface temperature anomalies that fluctuate almost in phase with the centennial TSI variations exhibiting a correlation coefficient of about $r = 0.53$, which however is not statistically robust as the overlying negative centennial trend and the high autocorrelation in the time scales considered reduces considerably the degrees of freedom of the filtered time series, as calculated following Zwiers and von Storch (1995). It must be noted that the maximum correlation is obtained at a time lag of 15–20 years, as expected by the slow ocean response. The regression coefficient is found to be 0.06 K per 1 W m^{-2} increase of TSI at lag 20 years, which is comparable to the sensitivity of 0.03–0.16 K per 1 W m^{-2} increase of TSI documented for the CMIP5 historical simulations (Misios *et al* 2016).

As indicated in figure 1, global mean precipitation in CESM-LME and likewise PDRMIP (not shown) scales linearly to the global mean surface temperature. This allows us to express hydrological sensitivities in terms of a linear regression in all four experiments following the methodology of Gregory *et al* (2004). In the PDRMIP simulations the rapid and slow precipitation responses are separated by calculating the

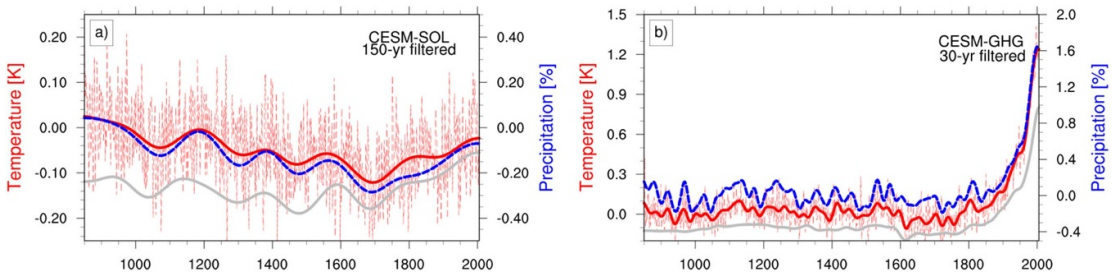


Figure 1. Filtered global mean temperature (red) and precipitation (blue) in the ensemble mean CESM-SOL and CESM-GHG over the period 850–2005. Low-pass filters of 150 years and 30 years have been applied in the CESM-SOL and CESM-GHG, respectively. Unfiltered ensemble mean temperature anomalies are superimposed as thin dotted curves. Precipitation is expressed in % relative to the climatology in the unforced control simulation. Changes in solar and GHG forcings are shown in grey and plotted with an arbitrary scaling to facilitate illustration.

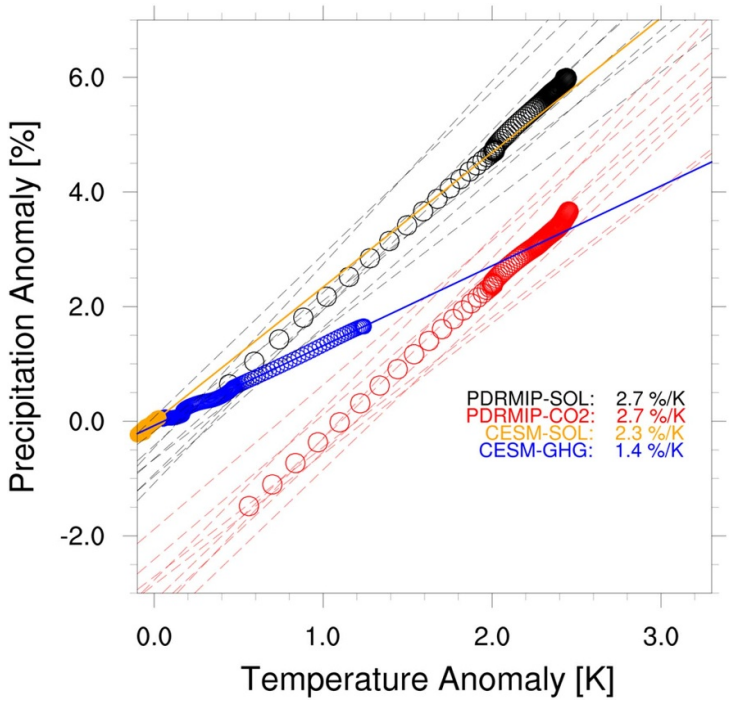


Figure 2. Scatter plot of filtered annual global mean precipitation versus temperature in the PDRMIP-SOL (black circles), PDRMIP-CO_2 (red circles), CESM-SOL (orange circles, period 850–2005) and CESM-GHG (blue circles, period 1850–2005) simulations. Solid lines (orange and blue) indicate slopes for CESM-SOL and CESM-GHG (2.3% K^{-1} and 1.4% K^{-1}). The multi-model mean slope is 2.7% K^{-1} for both PDRMIP simulations. Black and red dashed lines indicate the slope of each individual model in the PDRMIP ensemble.

intercept and slope, respectively, between ensemble mean filtered precipitation and surface temperature, while in the transient simulations of CESM-LME, regression coefficients isolate the apparent (total) hydrological sensitivity, given that it is not possible to separate the rapid and slow responses in these type of simulations (Flaschner *et al* 2016). Previous studies of PDRMIP simulations have analysed composite anomalies in terms of the last 50 years versus unperturbed conditions, but the results are generally consistent regardless of the method (Samset *et al* 2016).

Figure 2 shows the scatter of filtered global mean precipitation versus surface temperature in PDRMIP-SOL and PDRMIP-CO_2 (black and red circles, respectively). In the first year, both ensembles exhibit a surface warming of 0.5 K. In PDRMIP-CO_2 there is a corresponding reduction in precipitation of about −1.6%, explained by the negative rapid adjustments, while PDRMIP-SOL shows negligible fast changes in global precipitation. The linear slope is about 2.7% K^{-1} in both PDRMIP-SOL and PDRMIP-CO_2 respectively, consistent with the estimates of slow hydrological sensitivity of 2.5% K^{-1} and 2.7% K^{-1} for CO_2 and solar forcing documented in Samset *et al* (2016). The slope in individual PDRMIP models (black and red dotted lines in figure 2) ranges from 3.2% K^{-1} to 2.3% K^{-1} in both experiments. Analysis of the CMIP5 simulations of quadrupling the CO_2 concentrations have found slow hydrological sensitivities of about 2.6–2.8% K^{-1} and

geoengineering experiments of reduced incoming radiation have found 2.7% K^{-1} (Sillmann *et al* 2017), similar to the PDRMIP-SOL. The fast temperature-independent precipitation change estimated by the intercept of the regression, is −0.61% for solar and −2.94% for CO_2 forcing, consistent with the expectation of a considerably stronger rapid adjustment to CO_2 perturbation (Andrews *et al* 2010, Samset *et al* 2016).

Global mean surface temperature in CESM-SOL varies by about 0.06 K following centennial variations in TSI (figure 1 and orange circles in figure 2), with evidence for a time lag of about 20 years for both global temperature and precipitation. We calculate a slope of 2.3% K^{-1} of global precipitation increase with the associated global warming over the period 850–2005, which is the apparent hydrological sensitivity according to the definition of Flaschner *et al* (2016). As expected, this sensitivity is slightly lower than the slow hydrological sensitivity of 2.8% K^{-1} inferred from an individual PDRMIP-SOL experiment that used a similar version of the NCAR-CESM1-CAM5 model that carried out the CESM-LME runs. In the case of CESM-GHG, the apparent hydrological sensitivity over the industrial period (1850–2005) is found to be 1.4% K^{-1}, considerably weaker than the slow hydrological sensitivity of PDRMIP-CO_2, explained by rapid adjustments to increased GHG concentrations and atmospheric opacity. We note that the apparent hydrological sensitivity in CESM-GHG will also depend on the historical variation in non-CO_2 GHGs. Methane, N_2O, and CFCs have been shown to have slightly higher apparent hydrological sensitivities than CO_2 (Hodnebrog *et al* 2020), so the CESM-GHG hydrological sensitivity is likely an upper bound.

The CESM simulations indicate that we should expect a stronger sensitivity of the global mean precipitation to the surface temperature in the preindustrial than the post-1850 period, for equal global mean warming, because precipitation responses in the later period are muted by the negative impact of the rapid adjustments. Liu *et al* (2013) reached a similar conclusion by considering the combined solar plus volcanic forcing in the pre-industrial period versus the GHG forcing which dominates over the industrial period and they documented sensitivities of 2.1% K^{-1} versus 1.4% K^{-1}, consistent with our findings. In the following we show that the solar forcing is also responsible for stronger responses at regional scales for equal increase in global mean temperature.

3.2. Regional responses

Previous analysis of the PDRMIP simulations have documented patterns of hydrological sensitivities that exhibit substantial magnitudes of almost 30% K^{-1} over the inter-tropical convergence zone (ITCZ) under the influence of CO_2 and TSI forcing (Samset *et al* 2018). Figure 3, which focuses in the Indo-Pacific region, identifies the strongest absolute changes over the equatorial Pacific, with magnitude exceeding 1 mm d^{-1} per 1 K increase of global mean temperature, irrespective of the forcing. The signal is significant with two-tailed p-values < 0.05 in most of the tropics. Outside the equator, a band of negative anomalies at 10° N is indicative of an equatorward shift of the ITCZ. This intensification of the regional precipitation pattern has been attributed to deviations in surface temperature gradients (Xie *et al* 2010) and thermodynamic considerations of increased atmospheric water vapour associated with a warmer surface and the associated increase of moisture convergence (Held and Soden 2006, Bony *et al* 2013).

CESM-SOL shows similar patterns of precipitation response to PDRMIP, providing additional confidence that the regressed signals in figure 3(c) can be genuinely attributed to TSI forcing and the associated surface warming. Like PDRMIP-SOL, excess rainfall is found in the western and central equatorial Pacific with peak sensitivity > 1 mm d^{-1} per 1 K increase of global mean temperature from centennial TSI forcing, with p-values <0.05 assuming one degree of freedom in the time series. Outside the equator, negative anomalies are simulated associated with an overall contraction of the ITCZ in solar maxima. This pattern is also detected in the CESM-GHG ensemble, albeit of reduced amplitude that is likely due to the muted global hydrological sensitivity under the influence of historical GHGs. Precipitation anomalies in figure 3(d) hardly exceeds 0.4 mm d^{-1} K^{-1} in the equatorial Pacific, which is less than half the sensitivity found for solar forcing. As surface warming continues to rise, it is expected that the slow temperature-related response will dominate over the rapid adjustments and eventually a clearer pattern should be detected in future GHG scenario simulations, as shown in recent CESM large-ensemble single forcing runs (Deser *et al* 2020) for the 1970–2019 period.

Using the forcing-dependent hydrological sensitivities from PDRMIP, Richardson *et al* (2018) reached a similar conclusion and show that 20th century precipitation changes over the oceans have been suppressed by GHG rapid adjustments, but will become larger with future warming. By comparing responses in future versus present climate simulated with CMIP5 models, Liu *et al* (2013) also identified similar patterns of increased precipitation over the Pacific.

The pattern of precipitation anomalies identified in the PDRMIP and CESM-SOL is associated with a warmer Pacific (contours in figure 3), that is stronger in the east than the west. A similar pattern of ocean warming in the Pacific has been found in the composite analysis of the PDRMIP models of Samset *et al* (2018). The regression pattern is characterized by a reduced zonal temperature gradient

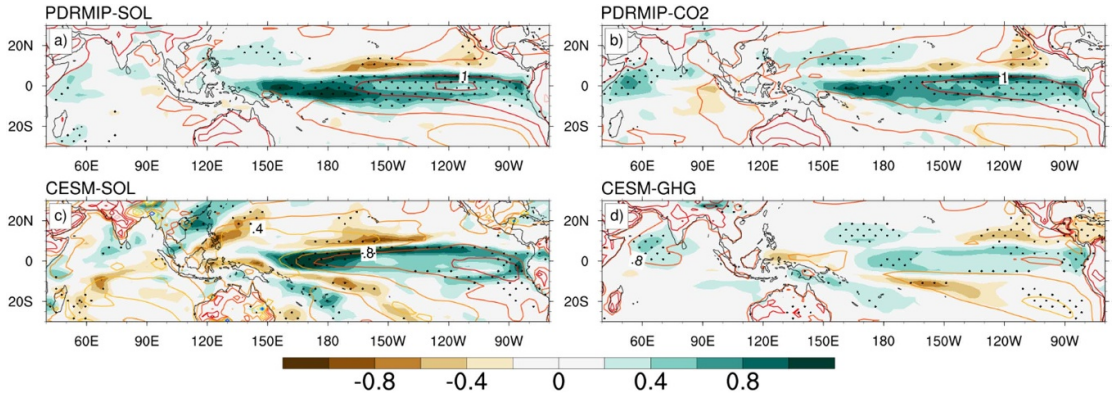


Figure 3. Spatial patterns of ensemble mean filtered precipitation (shaded, in mm d^{-1} K^{-1}) and surface temperature (contours, in K K^{-1}) regressed onto the filtered global mean surface temperature in (a) PDRMIP-SOL, (b) PDRMIP-CO_2, (c) CESM-SOL and (d) CESM-GHG simulations. Stippling indicates regions of chance probability $p < 0.05$ with a t-test assuming one degree of freedom calculated following Zwiers and von Storch (1995). Contour spacing is 0.2 K K^{-1}.

resembling a positive ENSO phase, although the detected signals refer to multidecadal (>30 years) time scales. This leads to an eastward shift of the convective precipitation that brings more rainfall to the central Pacific. In contrast, CESM-GHG does not show any clear evidence for stronger warming in the eastern equatorial Pacific (figure 3(d)), as expected from its weaker precipitation sensitivity over the 1850–2005 period. Deser *et al* (2020), however, demonstrated a pattern of amplified warming in the tropical Pacific of increasing magnitude over the last century, particularly after 1970s when the GHG forcing dominates, in an ensemble of CESM simulations spanning the 1920–2019 period.

We examined the robustness of the solar signatures in figure 3(c) by calculating differences of unfiltered time series between the periods of the Medieval Climate Anomaly (MCA) and Little Ice Age (LIA) which coincide with the grand solar maxima and grand solar minima. To make results comparable with Liu *et al* (2013), MCA is defined as the period 1100–1200 and LIA spans over the 1630–1730 period, although different definitions are possible. The LIA is the coldest period in the CESM-SOL, suggesting that the Maunder minimum of the solar activity reduced global mean surface temperature by about 0.1 K compared to the MCA period. We note though that the simulated response is much weaker than estimates based on proxy data, suggesting that additional cooling from volcanic eruptions and land use changes is needed to explain the observed magnitudes (Otto-Bliesner *et al* 2015). As in figure 3(c), the pattern of precipitation anomalies in the tropical pacific between MCA and LIA is characterized by wetter conditions in the equatorial Pacific, with the strongest positive anomalies of 0.2 mm d^{-1} found in the central region (supplementary figure 2). Likewise, the Pacific is generally warmer by about 0.1 K in MCA in comparison to LIA, in agreement with the analysis of all forcing CESM ensemble (Otto-Bliesner *et al* 2015).

3.3. Sensitivity of the Walker circulation

Precipitation responses in the tropical Pacific are highly dependent on changes in the Walker circulation, which is strongly sensitive to variations in sea surface temperature (SST) gradients. Several studies have provided evidence that the Pacific Walker circulation weakens with increasing CO_2 (Held and Soden 2006, Vecchi *et al* 2006) and a weakened Walker circulation has also been attributed to warming in the tropical SSTs (Tokinaga *et al* 2012). Likewise, there is an observational and modelling evidence that the 11 year solar cycle forcing might slow down the Walker circulation (Misios *et al* 2019). Our analysis of the PDRMIP simulations finds a similar reduction of the Walker circulation in response to TSI and CO_2. Interestingly, both PDRMIP-SOL and PDRMIP-CO_2 simulate positive anomalies of the filtered equatorial (10° S–10° N) zonal winds over the Pacific, suggesting an overall reduction of the climatological easterlies (figure 4). The strongest sensitivity of 0.4 m s^{-1} K^{-1} and 0.6 m s^{-1} K^{-1} to solar and CO_2 respectively is found around 600–800 hPa 140° E–180° E, while winds at 200 hPa form a dipole of positive and negative anomalies further corroborating the notion of an eastward shift of the Walker Circulation. Following the previous convention for scale separation of the precipitation response, we term this pattern as the temperature dependent response of the Walker circulation, which is similar for both CO_2 and TSI forcing. We note large differences in the simulated pattern of tropical wind anomalies among the PDRMIP models, but in any individual model, TSI and CO_2 forced patterns are strikingly similar (supplementary figure 3). This means that structural differences among the climate models contribute to the uncertainty of the Walker circulation response and not the nature of the applied forcing.

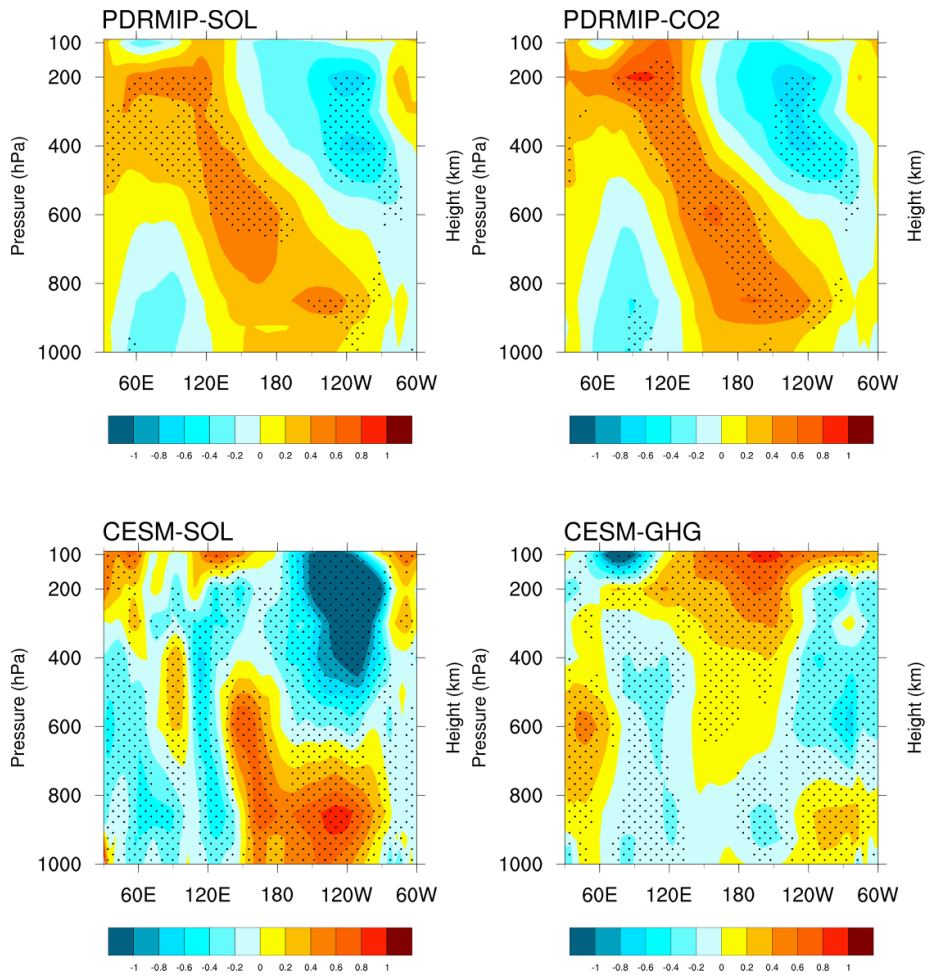


Figure 4. Spatial patterns of ensemble mean filtered equatorial (5° S–5° N) winds (m s^{-1} K^{-1}) regressed onto the filtered global mean surface temperature in (a) PDRMIP-SOL, (b) PDRMIP-CO_2, (c) CESM-SOL and (d) CESM-GHG simulations. Stippling indicates regions of chance probability $p < 0.05$ with a t-test assuming four degrees of freedom to account for the autocorrelation of the filtered time series.

Comparison of the CESM-SOL and PDRMIP-SOL results shows that variations of TSI at centennial time scales cause similar changes in the Walker circulation. Figure 4(c) shows westerly anomalies in the western and central Pacific up to 600 hPa, paired with negative anomalies at 200 hPa between 160° W and 80° W, which resembles the response simulated in the ensemble mean PDRMIP-SOL. As with PDRMIP, the strongest sensitivities occur in the central Pacific around 600–800 hPa, with a slightly larger maximum sensitivity of 0.8 m s^{-1} K^{-1} (figure 4(c)). CESM-GHG on the other hand, does not support the evidence of PDRMIP-CO_2 for a reduction of the Walker circulation. This is consistent with the response of the ocean temperatures, which in CESM-GHG is weaker than in CESM-SOL and lacks the stronger warming in the eastern pacific, a response that has been identified in all other ensemble simulations.

It has been suggested that excess surface heating in the extra-tropics is subducted into the tropics affecting the upwelled water in the eastern equatorial cold tongue (Gu and Philander 1997). The multi-decadal time scale of this oceanic 'tunnel' is relevant to the centennial variations examined here and our regression analysis identifies similar bands of surface warming in the extratropical Pacific, being stronger over the South Ocean (not shown). A reduced east–west temperature gradient along the equator should weaken the sea level pressure gradient, which in turn would slow down surface winds and the Walker circulation. In parallel with the dynamical ocean response, the Walker circulation might also slow down in solar maxima by the muted hydrological mechanism of Held and Soden (2006), as demonstrated in the model simulations of Misios *et al* (2019). Both PDRMIP and CESM runs do not provide any evidence for the 'dynamical ocean thermostat' mechanism, which is expected to enhance zonal SST gradient in the equatorial Pacific (Clement *et al* 1996). This proposed mechanism would strengthen precipitation over the maritime continent, strengthen surface easterlies and ultimately accelerates the Walker circulation, in contrast to the responses seen in figures 3 and 4.

We note that the CESM-LME ensemble is based on the CESM1-CAM5, which shows the strongest sensitivity of the Walker circulation in the PDRMIP runs (supplementary figure 3). For this reason, a possible overestimation of solar cycle signatures in the CESM-SOL cannot be excluded per se and this may explain the generally stronger sensitivities in precipitation and winds simulated with the CESM-SOL. However, here we do not aim to provide a quantitative assessment of the solar influence on the Walker circulation, but highlight similarities and differences in the precipitation and circulation responses in the Indo-Pacific to the TSI and GHG forcings.

4. Discussion and summary

Previous analysis of last millennium simulations have suggested that periods of high solar forcing increase SST gradients in the equatorial Pacific Ocean and decrease rainfall, while increasing GHG concentrations have the opposite effect (Mann *et al* 2009, Liu *et al* 2013). Proxy reconstructions of surface temperature have also suggested a cooling in the equatorial Pacific during the MCA that coincided with elevated solar activity, but model simulations do not provide support for such a La-Nina like response (Otto-Bliesner *et al* 2015). In contrast, the CESM-LME simulations provide evidence that solar and GHG forcings cause very similar patterns in the tropical Pacific characterized by an ocean warming, enhanced precipitation in the central Pacific, and a weakening and eastward shift of the Walker circulation. Moreover, CESM-SOL indicates that the period of MCA is characterized by positive SSTs under the sole influence of solar forcing (and vice versa during the solar minimum period of the LIA). The inclusion of idealized single-forcing simulations from nine different PDRMIP models further supports this conclusion, which differs from previous studies that have typically relied on all-forcing last millennium simulations—meaning that the solar cycle response could not be cleanly separated from volcanic forcing which also varied over the same time period—or relied on a single model's results. A climate model intercomparison of the last millennium simulations has also demonstrated substantial discrepancies in estimations of the Pacific temperature change during MCA, highlighting the potential role of internal variability (Fernández-Donado *et al* 2013). Hence, our result cannot be extrapolated directly to explain proxy records in the historical periods, as other forcing agents and natural variability likely play a significant role (Tan *et al* 2019). Despite this, reconstructions of rainfall variations in the Central Pacific provide some evidence for increased precipitation during the MCA associated with an eastward shift of the Walker circulation (Tan *et al* 2019), in qualitative agreement with the response shown in figures 3 and 4.

By analysing the transient CESM simulations we confirm previous findings that for the same amount of global warming we should expect a stronger hydrological sensitivity to solar than GHG forcing, because rapid adjustments to GHG forcing mute the slow temperature-dependent response. This result implies that tropical climate could be more susceptible to solar variability than to GHG variations during the pre-industrial period, given comparable global mean temperature changes. However, as the GHG forcing increases in the 20th century and dominates in the last decades and in the future (Deser *et al* 2020), we expect a small contribution of the TSI in future changes in tropical precipitation and circulation, even under prolonged solar minimum conditions (Meehl *et al* 2013). The similarity of the TSI and GHG tropical precipitation responses is analogous to the similarity of the patterns (but opposite sign) in response to anthropogenic aerosols and GHG over the 2nd half of the 20th century, demonstrating that a common set of coupled air-sea processes is fundamental to pattern formation in response to different forcing agents (Deser *et al* 2020).

The collective analysis of CESM and PDRMIP simulations provides qualitative support to the observational evidence for a slowdown of the Walker circulation and enhanced precipitation in the Central pacific (Misios *et al* 2019), but the role of internal variability needs to properly assessed by considering large ensemble simulations. The regression coefficients calculated in PDRMIP-SOL and CESM-SOL imply that in reality we should expect miniscule changes in precipitation and wind anomalies in response to the 11 year solar cycle because the observed global mean surface warming to the 11 year solar cycle barely exceeds 0.1 K. This raises questions on the detectability of solar cycle signatures in the tropical Pacific in the observational records. However, we note the possibility that (a) CESM might not capture the relative contribution of the mechanisms that have been suggested to amplify solar responses in the Tropical Pacific and/or (b) some mechanisms may operate on decadal but not multi-decadal time scales.

To the extent that CESM-LME simulations are a valid representation of past climate variability, we suggest that the solar and GHG forcing on multi-decadal timescales have caused similar spatial patterns of forced response in Pacific, characterized by a weaker Walker circulation, positive SST anomalies and enhanced precipitation in the western/central equatorial Pacific. Given the possible interference between different competing mechanisms that operate on different time scales, future research should focus on disentangling their relative role with carefully designed idealized simulations.

Data availability statement

The data that support the findings of this study are available upon reasonable request from the authors.

Acknowledgments

The authors thank three anonymous reviewers and the editorial team for constructive comments on the manuscript. The research is funded by the project 'Cosmic and electric effects on aerosols and clouds' (MIS: 5049552) under the call for proposals 'Support for researchers with emphasis on young researchers—Cycle B' (EDULL 103). The project is co-financed by Greece and the European Union (European Social Fund (ESF)) by the Operational Programme Human Resources Development, Education and Lifelong Learning 2014-2020. LG acknowledges support by the UK Natural Environment Research Council (NERC) through Grant NE/N010965/1 and the NERC National Centre for Atmospheric Science (NCAS). SM acknowledges the Villum Foundation Experiment Programme 'Environmental consequences of solar cosmic rays'. The authors are also grateful to Øivind Hodnebrog and Olivier Boucher who provided advice on the manuscript, and to the whole PDRMIP modelling team for making their data available.

ORCID iDs

Stergios Misios https://orcid.org/0000-0003-1226-4719
Matthew Kasoar https://orcid.org/0000-0001-5571-8843
Lesley Gray https://orcid.org/0000-0002-7803-9277
Joanna Haigh https://orcid.org/0000-0001-5504-4754
Stavros Stathopoulos https://orcid.org/0000-0001-8685-328X
Konstantinos Kourtidis https://orcid.org/0000-0002-5753-7074
Gunnar Myhre https://orcid.org/0000-0002-4309-476X
Drew Shindell https://orcid.org/0000-0003-1552-4715

References

Allan R P *et al* 2020 Advances in understanding large-scale responses of the water cycle to climate change *Ann. New York Acad. Sci.* **1472** 49–75
Allen M R and Ingram W J 2012 Constraints on future changes in climate and the hydrologic cycle (vol 419, pg 224, 2002) *Nature* **489** 590
Andrews T, Forster P M, Boucher O, Bellouin N and Jones A 2010 Precipitation, radiative forcing and global temperature change *Geophys. Res. Lett.* **37** L14701
Bala G, Caldeira K and Nemani R 2010 Fast versus slow response in climate change: implications for the global hydrological cycle *Clim. Dyn.* **35** 423–34
Bayr T, Dommenget D, Martin T and Power S 2014 The eastward shift of the Walker Circulation in response to global warming and its relationship to ENSO variability *Clim. Dyn.* **43** 1–17
Bony S, Bellon G, Klocke D, Sherwood S, Fermepin S and Denvil S 2013 Robust direct effect of carbon dioxide on tropical circulation and regional precipitation *Nat. Geosci.* **6** 447–51
Chiodo G and Polvani L M 2016 Reduction of climate sensitivity to solar forcing due to stratospheric ozone feedback *J. Clim.* **29** 4651–63
Chou C, Neelin J D, Chen C A and Tu J Y 2009 Evaluating the 'Rich-Get-Richer' mechanism in tropical precipitation change under global warming *J. Clim.* **22** 1982–2005
Chung E-S, Timmermann A, Soden B J, Ha K-J, Shi L and John V O 2019 Reconciling opposing Walker circulation trends in observations and model projections *Nat. Clim. Change* **9** 405–12
Clement A C, Seager R, Cane M A and Zebiak S E 1996 An ocean dynamical thermostat *J. Clim.* **9** 2190–6
Collins M *et al* 2010 The impact of global warming on the tropical Pacific ocean and El Nino *Nat. Geosci.* **3** 391–7
Deser C, Phillips A S, Simpson I R, Rosenbloom N, Coleman D, Lehner F, Pendergrass A G, Dinezio P and Stevenson S 2020 Isolating the evolving contributions of anthropogenic aerosols and greenhouse gases: a new CESM1 large ensemble community resource *J. Clim.* **33** 7835–58
Dinezio P N, Clement A C, Vecchi G A, Soden B J and Kirtman B P 2009 Climate response of the equatorial pacific to global warming *J. Clim.* **22** 4873–92
Dinezio P N, Clement A, Vecchi G A, Soden B, Broccoli A J, Otto-Bliesner B L and Braconnot P 2011 The response of the Walker circulation to last glacial maximum forcing: implications for detection in proxies *Paleoceanography* **26** PA3217
Fernández-Donado L *et al* 2013 Large-scale temperature response to external forcing in simulations and reconstructions of the last millennium *Clim. Past* **9** 393–421
Flaschner D, Mauritsen T and Stevens B 2016 Understanding the intermodel spread in global-mean hydrological sensitivity *J. Clim.* **29** 801–17
Gray L *et al* 2010 Solar influences on climate *Rev. Geophys.* **48** RG4001
Gregory J M, Ingram W J, Palmer M A, Jones G S, Stott P A, Thorpe R B, Lowe J A, Johns T C and Williams K D 2004 A new method for diagnosing radiative forcing and climate sensitivity *Geophys. Res. Lett.* **31** L03205
Gu D and Philander S G H 1997 Interdecadal climate fluctuations that depend on exchanges between the tropics and extratropics *Science* **275** 805
Haigh J D 1994 The role of stratospheric ozone in modulating the solar radiative forcing of climate *Nature* **370** 544–6
Harder J W, Béland S and Snow M 2019 SORCE-based solar spectral irradiance (SSI) record for input into chemistry-climate studies *Earth Space Sci.* **6** 2487–507
He J and Soden B J 2015 Anthropogenic weakening of the tropical circulation: the relative roles of direct CO_2 forcing and sea surface temperature change *J. Clim.* **28** 8728–42
Heede U K, Fedorov A V and Burls N J 2020 Time scales and mechanisms for the tropical pacific response to global warming: a tug of war between the ocean thermostat and weaker walker *J. Clim.* **33** 6101–18
Held I M and Soden B J 2006 Robust responses of the hydrological cycle to global warming *J. Clim.* **19** 5686–99
Hodnebrog Ø, Aamaas B, Fuglestvedt J S, Marston G, Myhre G, Nielsen C J, Sandstad M, Shine K P and Wallington T J 2020 Updated global warming potentials and radiative efficiencies of halocarbons and other weak atmospheric absorbers *Rev. Geophys.* **58** e2019RG000691

Huneeus N *et al* 2014 Forcings and feedbacks in the GeoMIP ensemble for a reduction in solar irradiance and increase in CO_2 *J. Geophys. Res.* **119** 5226–39

Kohyama T, Hartmann D L and Battisti D S 2017 La Nina-like mean-state response to global warming and potential oceanic roles *J. Clim.* **30** 4207–25

L'heureux M L, Lee S and Lyon B 2013 Recent multidecadal strengthening of the Walker circulation across the tropical Pacific *Nat. Clim. Change* **3** 571–6

Liu J, Wang B, Cane M A, Yim S-Y and Lee J-Y 2013 Divergent global precipitation changes induced by natural versus anthropogenic forcing *Nature* **493** 656

Mann M E 2004 On smoothing potentially non-stationary climate time series *Geophys. Res. Lett.* **31** L07214

Mann M, Zhang Z H, Rutherford S, Bradley R S, Hughes M K, Shindell D, Ammann C, Faluvegi G and Ni F B 2009 Global signatures and dynamical origins of the Little Ice Age and Medieval Climate Anomaly *Science* **326** 1256–60

Meehl G A, Arblaster J M and Marsh D R 2013 Could a future 'Grand Solar Minimum' like the Maunder Minimum stop global warming? *Geophys. Res. Lett.* **40** 1789–93

Meehl G A, Arblaster J M, Matthes K, Sassi F and van Loon H 2009 Amplifying the pacific climate system response to a small 11-year solar cycle forcing *Science* **325** 1114–8

Misios S *et al* 2016 Solar signals in CMIP-5 simulations: effects of atmosphere-ocean coupling *Q. J. R. Meteorol. Soc.* **142** 928–41

Misios S, Gray L J, Knudsen M F, Karoff C, Schmidt H and Haigh J 2019 Slowdown of the Walker circulation at solar cycle maximum *Proc. Natl Acad. Sci.* **116** 7186–91

Mitchell D M *et al* 2015 Solar signals in CMIP-5 simulations: the stratospheric pathway *Q. J. R. Meteorol. Soc.* **141** 2390–403

Myhre G *et al* 2016 PDRMIP: a precipitation driver and response model intercomparison project—protocol and preliminary results *Bull. Am. Meteorol. Soc.* **98** 1185–98

Myhre G *et al* 2018 Quantifying the importance of rapid adjustments for global precipitation changes *Geophys. Res. Lett.* **45** 11,399–11,405

O'gorman P A, Allan R P, Byrne M P and Previdi M 2012 Energetic constraints on precipitation under climate change *Surv. Geophys.* **33** 585–608

Otto-Bliesner B L, Brady E C, Fasullo J, Jahn A, Landrum L, Stevenson S, Rosenbloom N, Mai A and Strand G 2015 Climate variability and change since 850 CE: an ensemble approach with the community earth system model *Bull. Am. Meteorol. Soc.* **97** 735–54

Richardson T B *et al* 2018 Drivers of precipitation change: an energetic understanding *J. Clim.* **31** 9641–57

Samset B H *et al* 2016 Fast and slow precipitation responses to individual climate forcers: a PDRMIP multimodel study *Geophys. Res. Lett.* **43** 2782–91

Samset B H *et al* 2018 Weak hydrological sensitivity to temperature change over land, independent of climate forcing *npj Clim. Atmos. Sci.* **1** 20173

Shindell D T, Faluvegi G and Schmidt G A 2020 Influences of solar forcing at ultraviolet and longer wavelengths on climate *J. Geophys. Res.* **125** e2019JD031640

Sillmann J, Stjern C W, Myhre G and Forster P M 2017 Slow and fast responses of mean and extreme precipitation to different forcing in CMIP5 simulations *Geophys. Res. Lett.* **44** 6383–90

Tan L C *et al* 2019 Rainfall variations in central Indo-Pacific over the past 2,700 y *Proc. Natl Acad. Sci. USA* **116** 17201–6

Tokinaga H, Xie S-P, Deser C, Kosaka Y and Okumura Y M 2012 Slowdown of the Walker circulation driven by tropical Indo-Pacific warming *Nature* **491** 439–43

Vecchi G A, Soden B J, Wittenberg A T, Held I M, Leetmaa A and Harrison M J 2006 Weakening of tropical Pacific atmospheric circulation due to anthropogenic forcing *Nature* **441** 73–76

Xie S-P, Deser C, Vecchi G A, Ma J, Teng H and Wittenberg A T 2010 Global warming pattern formation: sea surface temperature and rainfall *J. Clim.* **23** 966–86

Zhang B and Soden B J 2019 Constraining climate model projections of regional precipitation change *Geophys. Res. Lett.* **46** 10522–31

Zwiers F W and von Storch H 1995 Taking serial correlation into account in tests of the mean *J. Clim.* **8** 336–51